nature structural & molecular biology

# Mechanics of Hsp70 chaperones enables differential interaction with client proteins

Rainer Schlecht[1,3], Annette H Erbse[1–3], Bernd Bukau[1] & Matthias P Mayer[1]

**Hsp70 chaperones interact with a wide spectrum of substrates ranging from unfolded to natively folded and aggregated proteins. Structural evidence suggests that bound substrates are entirely enclosed in a β-sheet cavity covered by a helical lid, which requires structural rearrangements including lid opening to allow substrate access. We analyzed the mechanics of the lid movement of bacterial DnaK by disulfide fixation of lid elements to the β-sheet and by electron paramagnetic resonance spectroscopy using spin labels in the lid and β-sheet. Our results indicate that the lid-forming helix B adopts at least three conformational states and, notably, does not close over bound proteins, implying that DnaK does not only bind to extended peptide stretches of protein substrates but can also accommodate regions with substantial tertiary structure. This flexible binding mechanism provides a basis for the broad spectrum of substrate conformers of Hsp70s.**



Hsp70 chaperones play a dominant role in the cellular system that controls conformational states of proteins. A major feature attributing to this role is the ability of Hsp70s to function in regulated interactions with a large spectrum of protein clients that have conformers ranging from extended nascent polypeptides to fully assembled protein oligomers and aggregates[1,2]. This broad spectrum of client conformers is, however, difficult to reconcile with the mode of substrate interaction that is considered to be fairly simple and invariant.

Client binding occurs through the transient association of short hydrophobic segments with the C-terminal substrate-binding domain (SBD)[1–5]. This interaction is allosterically regulated by the N-terminal nucleotide-binding domain (NBD), whereby the conformation of the SBD changes between at least two states in a nucleotide-dependent manner[6]. Substrate trapping in a complex with Hsp70 requires ATP hydrolysis in a process that is synergistically stimulated by substrate binding and the activity of J-domain–containing cochaperones, which have a dual function to target substrates to Hsp70 and to stimulate ATP hydrolysis[7–9].

The crystal structure of the SBD of the *Escherichia coli* Hsp70 homolog DnaK (residues 389–607) in complex with a heptamer substrate peptide[10] revealed a unique assembly of two subdomains (**Fig. 1**). The first is a two-layer twisted β sandwich (residues 389–507) with four upward protruding loops that enclose the substrate peptide. The second is an α-helical subdomain (residues 508–607), which packs (through helix A and the proximal part of helix B) against the inner loops ($L_{1,2}$ and $L_{4,5}$) of the β-sheet subdomain and forms a lid-like structure over the substrate-binding cleft. The cocrystallized peptide is tightly encased by the substrate-binding pocket in an extended conformation. The helical lid seals in the substrate by forming a latch of a salt bridge and two hydrogen bonds to the outer loops ($L_{3,4}$ and $L_{5,6}$) (**Fig. 1a**). Subsequent NMR and crystal structures of SBDs from different Hsp70s showed essentially the same conformation emphasizing evolutionary conservation of the structure[11–16]. These structures, however, did not clarify whether in the absence of a peptide substrate the lid is tightly closed and how it opens to bind a substrate molecule. Most notable is the tight enclosure of the substrate peptide (**Fig. 1b**). Because of the size of the lid and the β-sheet subdomain, a folded protein would have to undergo extensive unfolding to accommodate a similar binding geometry in the Hsp70 substrate-binding cavity as the cocrystallized peptide[10]. Such a complete local unfolding of the DnaK-interacting substrates resulting in a minimal distance to the remainder of the protein of ≥10 Å is difficult to reconcile with the fact that the preferred binding sites for Hsp70s are stretches of hydrophobic residues, which are entropically disfavored in an aqueous environment.

To address these open questions, we introduced cysteine residues into the *E. coli* DnaK SBD such that possible opening movements were restricted. In addition, we used site-directed spin labeling combined with EPR spectroscopy, which enabled us to observe dynamic changes in the distance between the β subdomain and the helical lid when peptide or protein substrates were bound to the chaperone.

## RESULTS

### Probing the mechanics of SBD movements by disulfide bonds

Four models have been proposed for the ATP-induced opening of the substrate binding pocket of Hsp70 proteins: (i) unfolding of the middle part of helix B and kinking of its distal part, retaining close contacts between the β-sheet subdomain and helix A and the proximal part of helix B[10] (**Fig. 1c**, left); (ii) complete detachment of helix B and upward rotation[6] (**Fig. 1c**, middle left); (iii) sideward movement

[1]Zentrum für Molekulare Biologie der Universität Heidelberg (ZMBH), DKFZ–ZMBH Allianz, Im Neuenheimer Feld 282, Heidelberg, Germany. [2]Present address: Department of Chemistry and Biochemistry, University of Colorado Boulder, Boulder, Colorado, USA. [3]These authors contributed equally to this work. Correspondence should be addressed to M.P.M. (m.mayer@zmbh.uni-heidelberg.de) or B.B. (bukau@zmbh.uni-heidelberg.de).

Received 14 July 2010; accepted 14 December 2010; published online 30 January 2011; doi:10.1038/nsmb.2006

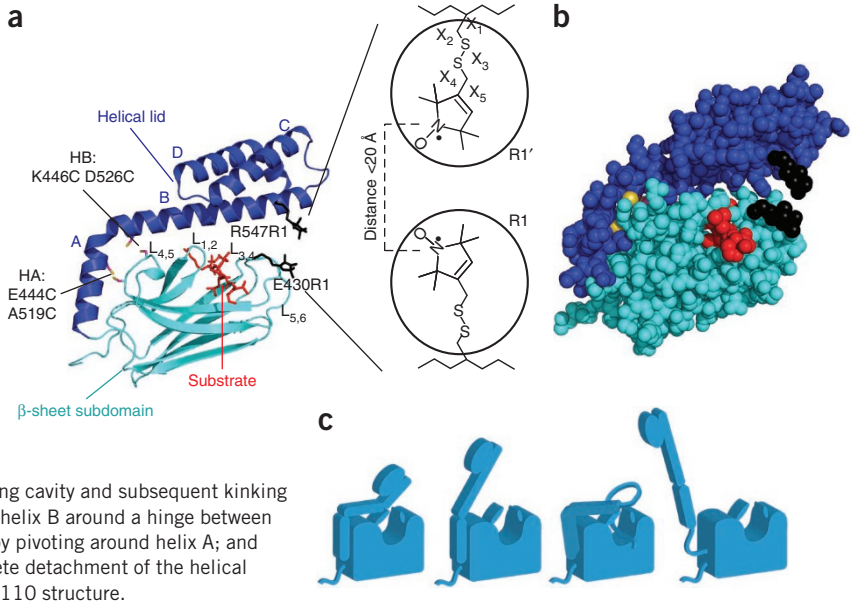


**Figure 1** Structure of the DnaK substrate-binding domain. (**a**) Illustration of E444C, A519C, K446C, D526C, E430R1 and R547R1′ alterations in the crystal structure of the SBD of DnaK (PDB 1DKX[10]) in cartoon representation. The β-sheet subdomain is drawn in cyan, the helical lid in blue and the cocrystallized substrate peptide NRLLTG in red. Modified residues are indicated. The E430R1,R547R1′ side chain pair in energy-minimized conformations are shown as stick models to illustrate the expected close proximity of the spin-labeled side chains in the 'closed lid' conformation. At right is the structure of the spin-labeled side chains illustrating the range (<20 Å) of detectable interactions[33]. Structural representations were created in PyMOL (http://www.pymol.org/). (**b**) A space-filling representation of the SBD shown in **a**. (**c**) Models of the proposed lid opening mechanisms: (left to right) (i) melting of helix B opposite the substrate-binding cavity and subsequent kinking of the C-terminal helical bundle; (ii) upward rotation of helix B around a hinge between helix A and helix B; (iii) sideward movement of the lid by pivoting around helix A; and (iv) formation of a continuous helix A and B and complete detachment of the helical subdomain from the β-sheet domain, similar to the Hsp110 structure.

of the lid by pivoting around helix A[13,16] (**Fig. 1c**, middle right); and (iv) formation of a continuous helix A and B and complete detachment from the β-sheet domain, similar to that seen in the Hsp110 structure[17] (**Fig. 1c**, right). To test these hypotheses, we introduced two pairs of cysteines into the substrate-binding domain of *E. coli* DnaK such that disulfide bond formation restricted the mobility of helix A or B (**Fig. 1a**). In a first variant, helix A can be linked to the β subdomain (E444C A519C; DnaK-HA), which should prevent any rotation around helix A and which prevents a complete detachment of the helical subdomain, as in the Hsp110 structure. In a second variant, the proximal part of helix B can be linked to the β subdomain (K446C D526C; DnaK-HB), which additionally prevents the upward rotation of the helical lid around a hinge between helices A and B (**Fig. 1c**, middle left). We then purified and oxidized the resulting mutant proteins. We confirmed quantitative disulfide bond formation by mass spectrometric analysis after modification of free cysteine side chains with sodium (2-sulfonatoethyl)methanethiosulfonate (MTSES) (**Supplementary Fig. 1**). DnaK-HA, once oxidized, could not be reduced by any reducing conditions tested. Therefore, we purified it in the presence of 20 mM DTT, and we performed all experiments in the presence of this high concentration of reducing agents to ensure the preservation of the reduced state. To verify structural integrity, we subjected oxidized and reduced proteins to thermal denaturation. We detected no structural defects by circular dichroism spectroscopy (**Supplementary Table 1**) and Fourier transform infrared spectroscopy (**Supplementary Fig. 2**), and the mutant variants were as stable as wild-type DnaK.

## Lid fixation does not inhibit substrate binding

To evaluate whether the restriction of conformational flexibility of the helical subdomain influences interaction with substrates, we first analyzed binding of a fluorescent peptide to oxidized and reduced DnaK double-cysteine mutants. In the absence of ATP, peptide substrate bound to both oxidized DnaK variants, DnaK-HA and DnaK-HB, as evidenced by fluorescence increase (data not shown). Peptide dissociation kinetics for both oxidized DnaK variants were similar to those for wild-type DnaK, demonstrating that the disulfide bridges do not prevent the opening of the substrate-binding pocket in the high-affinity state (**Fig. 2** and **Table 1**). In the reduced state, however, dissociation occurred more rapidly, with a 2- and 30-fold increased rate for DnaK-HA and DnaK-HB, respectively. The dramatic effect observed for DnaK-HB is most likely caused by the disruption of a network of ionic interactions stabilizing the interface between helices A and B and the β subdomain by the introduction of cysteine residues[18] (**Supplementary Fig. 3**). Upon disulfide bond formation, the interaction of the lid with the β subdomain may be stabilized, similar to the ionic interactions in the wild-type protein.

In the absence of ATP, peptide substrates associate to wild-type DnaK in a biphasic process because of a conformational equilibrium of the SBD of DnaK[19–21]. Reduced and oxidized DnaK-HA bound a peptide substrate with very similar kinetics as the wild-type protein (**Table 1**). In contrast, for reduced DnaK-HB, we observed a higher peptide association rate. Notably, for oxidized DnaK-HB, peptide association rates were similar to the wild-type protein; however, more peptide associated with the faster rate, arguing for an influence of the mutations on the conformation of the β subdomain of the DnaK SBD.

*In vivo*, the main substrates for DnaK are not peptides but rather partially folded and misfolded proteins. DnaK even binds some proteins in their native state, as, for example, the *E. coli* heat shock transcription factor $\sigma^{32}$, which was shown to be regulated by DnaK[22–24] and serves as a chaperone substrate *in vitro*[25–29]. Therefore, we analyzed the kinetic parameters of the interaction of wild-type DnaK and double-cysteine variants with radiolabeled $^{3}$H-$\sigma^{32}$ under both oxidizing and reducing conditions. We determined dissociation equilibrium and rate constants by gel filtration experiments, and these results are summarized in **Table 1**. Notably, the affinity for $\sigma^{32}$ was very similar for all DnaK variants tested under both oxidizing and reducing conditions (**Fig. 2** and **Table 1**). To show that the DnaK variants bound substrates specifically in the substrate-binding pocket, we combined the double-cysteine replacements with an amino acid exchange in the substrate-binding pocket demonstrated previously to block substrate binding (DnaK-V436F[30]; **Supplementary Fig. 4**). The V436F alteration reduced substrate binding to wild-type DnaK and double-cysteine variants alike, confirming that the interaction observed is a *bona fide* chaperone-substrate interaction. The determined dissociation rates and calculated association rates, however, were lower for both oxidized DnaK variants as compared to wild-type

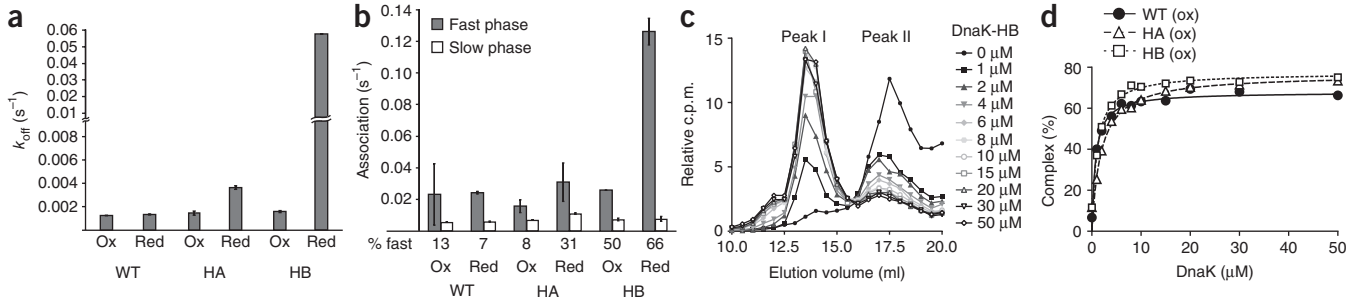


**Figure 2** DnaK variants show altered interaction with substrates. (**a**) Peptide substrates dissociated fastest from reduced DnaK-HB. Shown are unstimulated dissociation rate constants obtained for the dissociation of DNR peptide from oxidized or reduced DnaK wild-type or double cysteine variants (please note the break in the *y* axis). Fluorescence decay was fitted by a single exponential equation. (**b**) The reduced form of DnaK-HB showed the fastest association rate. Shown are apparent peptide association rates observed for the interaction of 0.5 µM DnaK with 2 µM DNR-peptide in a stopped-flow device. Rates for the fast (gray) and slow (white) phase and the amplitude of the fast phase (% fast) are given. Error bars represent the standard error of three independent experiments. (**c**) Elution profiles of gel filtration analysis over a Superdex 200 10/30 column (GE Healthcare). We incubated different concentrations of oxidized DnaK-HB (0–50 µM) with $^{3}$H-$\sigma^{32}$ (1 µM, 1,500 Bq) and separated the bound and unbound fractions by gel filtration. The amount of radio-labeled substrate protein is plotted against the elution volume. Peak I corresponds to the DnaK-$\sigma^{32}$ complex and peak II corresponds to free transcription factor. c.p.m., counts per minute. (**d**) Substrate affinity is not altered in DnaK double-cysteine mutants. Dissociation equilibrium titration of $^{3}$H-labeled $\sigma^{32}$ with 0–50 µM oxidized wild-type DnaK and double-cysteine variants. We determined the $K_d$ values by fitting the quadratic solution to the data (**Table 1**). Ox, oxidized.



DnaK, whereas we only detected slight differences for reduced DnaK-HA (**Table 1**). We observed the largest deviation from the wild-type protein for reduced DnaK-HB. The dissociation rate constant for $\sigma^{32}$ was ten times higher for this DnaK variant, consistent with the data for the peptide substrate. Taken together, the fixation of helix A and the proximal part of helix B does not prevent substrate binding but influences the dynamics of binding and release.

### Immobilization of the lid compromises chaperone activity

Because DnaK double-cysteine variants are able to bind protein substrates, we asked whether DnaK is functional in the refolding of chemically denatured firefly luciferase even with restricted lid mobility. Under reducing conditions (**Fig. 3a**), DnaK-HA can refold the denatured substrate with wild-type efficiency. In contrast, DnaK-HB does not support reactivation. Our findings suggest that the difference between wild type and DnaK-HB is because of the shorter retention of the substrate on the DnaK mutant caused by an increased dissociation rate.

Under oxidizing conditions, wild-type DnaK was able to recover only approximately 10% of the activity of native luciferase (**Fig. 3b**). As firefly luciferase contains four cysteine residues, trapping of non-functional protein conformations upon non-native disulfide-bond formation under oxidizing conditions is likely, which can explain the low yield of active protein. Notably, under these conditions, both DnaK-HA and -HB failed to reactivate luciferase even though they bind peptides and folded protein substrates with affinities similar to the wild-type protein. Because the disulfide bridge in DnaK-HA could not be reduced by DTT, we repeated luciferase refolding in the presence of DTT. Notably, even under these conditions, oxidized DnaK-HA was not able to refold luciferase (**Supplementary Fig. 5a**). To test whether this is a more general defect of the double-cysteine variants, we used a second widely used chaperone substrate, heat denatured malate dehydrogenase (MDH). Under reducing conditions, wild-type DnaK refolded MDH to almost 80% within 120 min (**Supplementary Fig. 5b**). DnaK-HA and DnaK-HB were able to refold MDH to 70% and 60%, respectively. MDH refolding results for DnaK-HB contrast those for the refolding of luciferase, indicating that different substrates have different requirements for association and dissociation kinetics. Under oxidizing conditions, wild-type DnaK refolded only about 25% of MDH within 120 min (**Supplementary Fig. 5c**). In contrast to the results for luciferase, DnaK-HA and DnaK-HB could refold some MDH but were clearly more compromised than wild-type DnaK.

### Alterations of allosteric control by helix A immobilization

The allosteric regulation of substrate binding by the nucleotide state is an essential feature of the chaperone activity of Hsp70s and is only poorly understood mechanistically. Therefore, we addressed whether fixation of helix A or the proximal part of helix B in oxidized DnaK variants affects the allosteric mechanism.

When added separately, the substrate protein $\sigma^{32}$ and the DnaJ cochaperone increase the low intrinsic ATPase activity of wild-type DnaK approximately 5- and 20-fold, respectively (**Fig. 4a**). Both proteins together synergistically stimulate ATP hydrolysis by two orders of magnitude to a rate of 0.08 $s^{-1}$. For oxidized DnaK-HB, the basal ATPase rate is already increased about fourfold. Addition of DnaJ stimulated this elevated ATPase rate further, but addition of $\sigma^{32}$ had little effect, and we observed no synergistic stimulation. These results argue for a defect in substrate-mediated stimulation of the ATPase activity. Upon reduction of the disulfide bond, the protein behaved almost like wild-type DnaK

**Table 1 Kinetic constants for DnaK-substrate interactions**

| | $\sigma^{32}$ | | | NR peptide (NRLLLTG) | | |
|---|---|---|---|---|---|---|
| | | | | | Association ($s^{-1}$) | |
| | $K_d$ (µM) | $k_{off}$ ($10^{-4}$ $s^{-1}$) | $k_{on}$ ($M^{-1}$ $s^{-1}$)[a] | $k_{off}$ ($10^{-3}$ $s^{-1}$) | Fast phase | Slow phase |
| DnaK (red) | 1.2 | 7.1 | 592 | 1.3 | 0.024 | 0.006 |
| DnaK-HA (red) | 0.69 | 6.6 | 956 | 3.6 | 0.031 | 0.011 |
| DnaK-HB (red) | 0.93 | 85.9 | 9,237 | 58 | 0.13 | 0.008 |
| DnaK (ox) | 0.86 | 8.5 | 988 | 1.2 | 0.023 | 0.006 |
| DnaK-HA (ox) | 2.2 | 2.0 | 91 | 1.8 | 0.016 | 0.007 |
| DnaK-HB (ox) | 1.3 | 3.8 | 292 | 1.8 | 0.026 | 0.008 |

[a] $k_{on}$ values were calculated from the $K_d$ and $k_{off}$ values. $K_d$, dissociation equilibrium constant; $k_{off}$, dissociation rate constant; $k_{on}$, association rate constant; ox, oxidized protein; red, reduced protein.

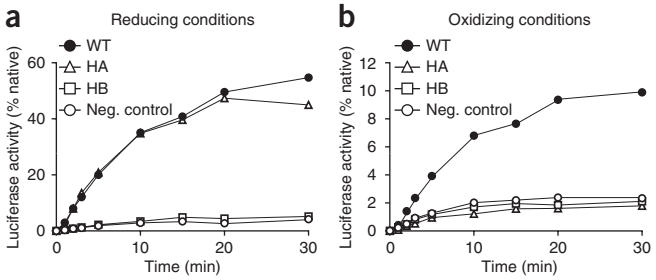


**Figure 3** Only reduced DnaK-HA is capable of refolding luciferase. (**a**–**b**) Refolding of chemically denatured firefly luciferase by wild-type DnaK and double-cysteine mutants under reducing (**a**) or oxidizing (**b**) conditions (80 nM luciferase, 800 nM DnaK, 160 nM DnaJ, 400 nM GrpE and 20 mM DTT for **a**). Luciferase activity is plotted as a fraction of the native luciferase control. Neg. control, negative control.

(**Fig. 4a**). Only synergistic stimulation was 2.5-fold lower than for wild-type DnaK, which could be due to a defect in the locking in of substrates into the binding pocket. Although reduced DnaK-HA behaves like wild-type protein, the disulfide-linked form shows a completely different behavior. The basal ATP hydrolysis rate is increased about ten times compared to wild-type DnaK but does not change at all upon addition of substrate and/or DnaJ.

To investigate the communication between the NBD and SBD further, we determined peptide dissociation rates in the presence of ATP (**Fig. 4b**). In wild-type DnaK, ATP binding leads to an opening of the substrate binding site, which increases the dissociation rate for the peptide substrate by three orders of magnitude[20,30]. Although both reduced double-cysteine mutants showed a slightly higher ATP-stimulated release rate, and oxidized DnaK-HB behaved like the wild-type protein, peptide dissociation from oxidized DnaK-HA was as just as slow as in the absence of ATP (compare to **Fig. 2**). In addition, we analyzed the coupling status of NBD and SBD by measuring the intrinsic fluorescence emission of the single tryptophan residue located in the NBD of DnaK, which undergoes an ATP-induced blueshift when the SBD is allosterically coupled[31,32]. In the reduced state, both DnaK variants showed a blueshift of 3–4 nm, similar to the value obtained for wild-type protein, arguing for functional interdomain coupling (**Fig. 4c**). However, when the proximal part of helix B was fixed to the β subdomain by oxidation, the maximum of tryptophan fluorescence shifted by only about 1 nm. This finding is consistent with the observation that the proximal part of helix B is required for the nucleotide-induced changes in fluorescence[32]. When helix A is fixed to the β subdomain, helix B should be free to interact with the NBD and induce a blueshift. However, we observed no changes in tryptophan fluorescence. Taken together, these findings show that mobility of the helical lid is a prerequisite for functional allosteric control of the Hsp70 cycle. In particular, a relocation of helix A relative to the β subdomain appears to be crucial.

### The helical lid does not close over protein substrates

Although the above experiments show that the proximal part of the helical lid can stay fixed with the β subdomain even when substrates are binding to DnaK, they do not provide information on the status of the distal part of the helical lid. We therefore investigated whether the helical lid closes completely even when folded protein substrates are bound, as suggested by the crystal structure of the DnaK-SBD–peptide complex[10]. For steric reasons, it is not possible to approach this issue by disulfide bridge formation. To investigate possible transitions between an open and a closed state of the distal part of helix B, we instead used EPR spectroscopy, which allowed us to monitor changes in the distance of paramagnetic centers induced by lid movement[33]. To this end, we introduced cysteine residues into the distal part of helix B and/or the outer loop $L_{3,4}$ of the β subdomain of DnaK, and we spin labeled these residues (DnaK-E430R1,R547R1′; **Fig. 1a**). First, we tested the effect of ATP binding on the spectrum of single- and double-labeled DnaK. EPR spectra in the absence (**Fig. 5a**, left) and presence (**Fig. 5a**, right) of ATP showed a clear difference when overlaid with the algebraic sum of the spectra of the corresponding single mutants (**Supplementary Fig. 6a**) normalized to the same number of spins. This sum represents the spectrum expected if the two labels were not interacting. For both spectra, we computed distance distributions[33] (**Fig. 5b** and **Supplementary Fig. 6b**). The distance distribution in the absence of nucleotide shows two interacting spin populations, one with an approximately 12 Å distance and one with a broader population between 16 Å and 20 Å. Only a small fraction of the label was not interacting (fraction of non-interacting spins, $f_{NI} = 0.09$), which is at a distance of more than 20 Å. Upon ATP addition, the short-distance population disappeared and almost 80% of the spin labels were separated by more than 20 Å, whereas in 20% of the molecules, the distance was in a range similar to the open form of the ADP-bound state.

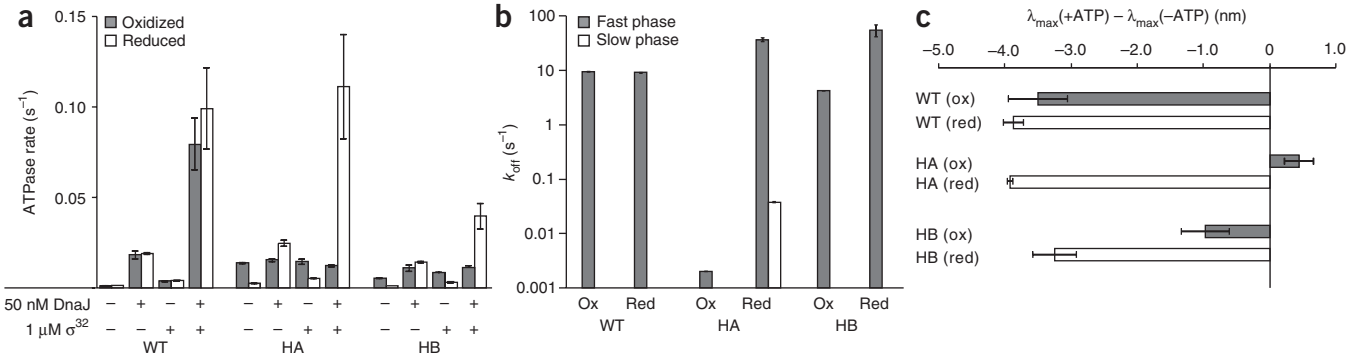


**Figure 4** Effects of disulfide bond formation on interdomain communication. (**a**) Restricting lid mobility alters basal and stimulated ATPase activity of DnaK. Single-turnover ATPase rates in the absence and presence of 50 nM DnaJ and 1 μM $\sigma^{32}$ under oxidizing (gray) and reducing conditions (white). (**b**) Oxidized DnaK-HA is impaired in ATP-stimulated peptide release. Peptide dissociation rates in the presence of ATP are shown. For reduced DnaK-HA, we observed a second phase (white bar). (**c**) Tryptophan fluorescence revealed defects in ATP-induced conformational changes in oxidized double-cysteine mutants. Difference of the wavelength of the emission maximum of tryptophan fluorescence in the presence of ATP minus the wavelength of the maximum in the absence of nucleotide. Reduced samples contain 20 mM DTT. Error bars represent the standard error of three independent experiments. Ox, oxidized; red, reduced.

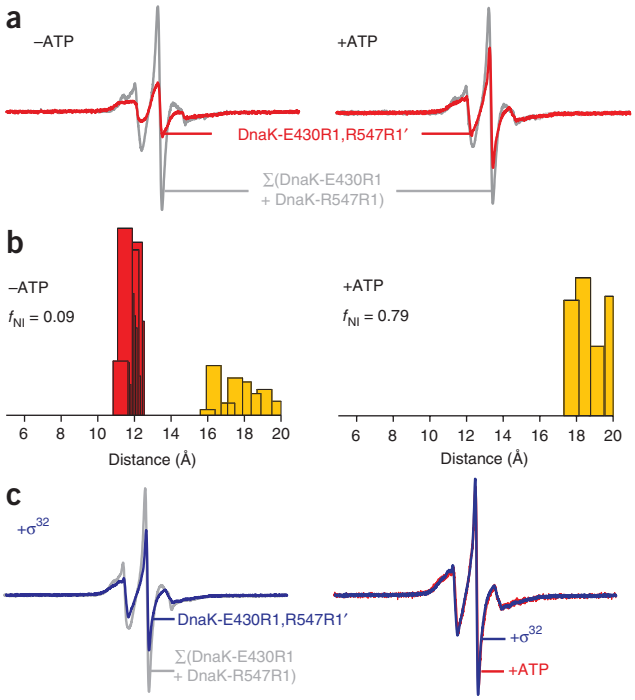


**Figure 5** EPR spectra of a spin pair in the SBD of DnaK in the presence of nucleotide and substrate. (**a**) Spectra of DnaK E430R1,R547R1′ (50 μM) in the absence (left) and presence (right) of ATP (2 mM) are shown. Comparison of the experimental spectrum of the double mutant (red line) with the algebraic sum of the spectra of the corresponding single mutants, normalized to the same number of spins (gray trace). (**b**) Derived interspin distance distribution between the spin pair in the absence and presence of ATP from fits to the spectra in **a** (**Supplementary Fig. 6b**). The *y* axis is arbitrary and chosen for the ease of presentation. The population of non-interacting spin pairs (distance > 20 Å) is not shown, but the fraction of total spin contributed to this population ($f_{NI}$) is given. (**c**) Investigation of the spin-spin interaction in the presence of the folded protein substrate $\sigma^{32}$ (300 μM). The left panel shows the comparison of the experimental spectrum of the double mutant (blue line) with the algebraic sum of the spectra of the corresponding single mutants (gray line) in the presence of bound protein, normalized to the same number of spins. The right panel shows an overlay of the experimental EPR spectrum of the double mutant in the presence of ATP (red line) with the spectrum of the mutant in the presence of $\sigma^{32}$ (blue line), illustrating that the spectrum of protein-substrate–bound DnaK is similar to the ATP bound, 'open lid' conformation.

To determine the effect of substrate binding on the spin-spin distance distribution, we first measured spectra of the labeled DnaK variant in the presence of the high-affinity peptide $\sigma^{32}$-M195–N207, which comprises the binding site of DnaK in native $\sigma^{32}$ (ref. 29) (**Supplementary Fig. 7a**). The spectra for peptide-bound and free DnaK-E430R1,R547R1′ in the absence of ATP overlay perfectly, indicating no changes in the distance distribution between the β sandwich and helical lid upon interaction with peptide substrates. The peptide had no effect on the spin-labeled single-cysteine variants (**Supplementary Fig. 7b**). To ensure that the spin-labels do not prevent substrate binding, we determined binding affinities of the fluorescently labeled peptide to DnaK with and without spin labels and found a difference of less than two-fold (**Supplementary Fig. 7c**).

As the cocrystallized peptide is tightly enclosed by the SBD (**Fig. 1b**), this raises the question of whether the SBD of DnaK binds native protein substrates in the same mode or, alternatively, whether the SBD has to assume a more open conformation in order to accommodate folded protein substrates. For these experiments, we used two *in vivo* substrates, $\sigma^{32}$ and the monomeric version of the F-plasmid replication initiator protein, RepE54 (ref. 34).

In contrast to the spectra for the peptide-bound DnaK, the spectra of the double spin-labeled DnaK in complex with $\sigma^{32}$ or RepE54 showed only little evidence of spin-spin interactions (**Fig. 5c** and **Supplementary Fig. 8b**, left panels) and had nearly identical line shapes compared to the spectrum of the ATP-bound 'open lid' conformation of the double mutant (**Fig. 5c** and **Supplementary Fig. 8b**, right panels), meaning that about 20% of the molecules were in a partially open state, and the remaining molecules showed a distance between spin labels of more than 20 Å. We took great care to exclude any contaminations with ATP in these experiments, and we checked all components for nucleotide content by HPLC. Although a protein substrate could affect the orientation of the spin labels in our EPR experiments, we could not detect changes in the spectra of the labeled single mutants upon substrate protein binding, indicating that the mobility of the spin probes was not altered by the presence of the substrate (**Supplementary Fig. 8a**,**c**). These results clearly indicate that binding of natively folded substrates forces the SBD of full-length DnaK to adopt an open conformation rather than to fully close and encase an extended stretch in the structure of the substrates. Although the distal part of helix B remains open when a protein substrate is bound, the disulfide bridge between the proximal part of helix B and the β subdomain can be closed even after protein binding (**Supplementary Fig. 9**).

Because the lid remains open when a protein substrate is bound, we wondered whether the lid adopts a position far removed from the bound substrate or whether the lid could interact with the substrate possibly as part of the chaperone function. Therefore, we attached a cross-linker to the distal part of helix B. **Figure 6** shows that a bound protein substrate can be cross-linked to helix B, indicating that the lid can approach the bound protein substrate to at least 10 Å.

## DISCUSSION

This study reveals new insights into the complex conformational dynamics of Hsp70 chaperones that control their interactions with substrates. The allosteric regulation by the nucleotide status of Hsp70 leads to an ATP-induced docking of the NBD and SBD and

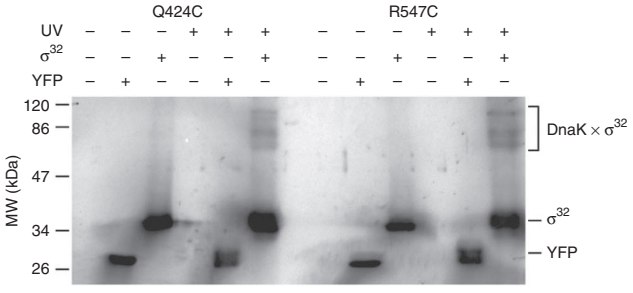


**Figure 6** The distal part of helix B can be cross-linked to bound substrate. We labeled DnaK-Q424C and DnaK-R547C with the heterobifunctional, thiol-specific, UV-inducible cross-linker 4-(2-Iodoacetamido)benzophenone (BPIA) and cross-linked to yellow fluorescent protein (YFP) and $\sigma^{32}$ by irradiation with UV light[39]. We visualized His-tagged substrates and cross-linking products by immunoblotting with a Penta-His Antibody (QIAGEN). Bands corresponding to DnaK-substrate complexes can be detected when BPIA is linked either to the β-sheet subdomain close to the substrate binding pocket (Q424C, compare to ref. 39) or to the distal part of helix B (R547C), however this is true only for the native substrate protein $\sigma^{32}$ and not for YFP, which is not bound by DnaK in its native state. MW, molecular weight.

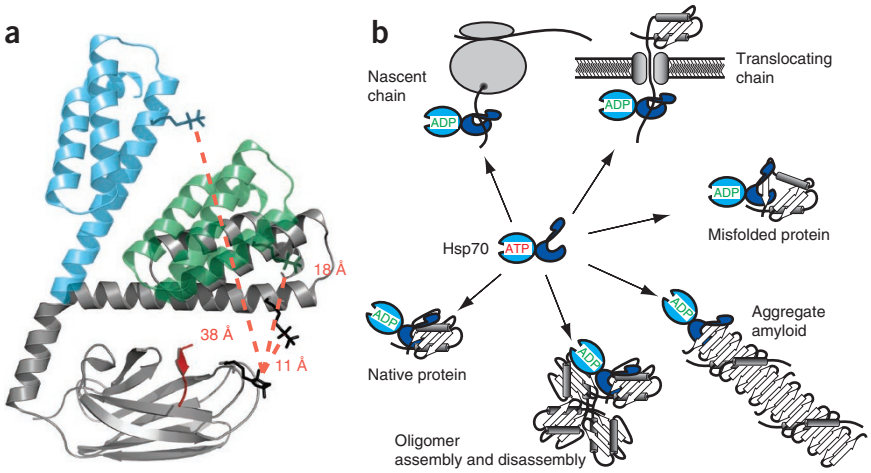


**Figure 7** Cartoon representation of the SBD of DnaK illustrating possible lid movements. (**a**) The 'closed lid' crystal structure is depicted as a dark gray cartoon and the R1 side chains as a dark gray stick model. The green translucent helical lid illustrates a distance of the nitroxide groups of the R1 moieties of 18 Å with a kinking of helix B opposite the substrate-binding pocket. The blue translucent lid visualizes a possible wide-open structure with a distance of 38 Å between the R1 groups. Because a distance of 38 Å is far beyond the detection range of dipolar spin-spin interactions with the method used, it remains unclear whether the lid actually opens to this extent. (**b**) Multiple functions of Hsp70 chaperones. Some are likely to allow lid closure, whereas others are rather unlikely to do so.

the burial of the hydrophobic linker connecting these domains[35,36]. These conformational changes trigger an opening of the β subdomain and a relocation of the helical lid of the SBD, processes which have remained poorly understood despite their decisive importance for Hsp70 function in protein folding. In the present study, we show that (i) no movement of the proximal part of helix B away from the inner loop $L_{4,5}$ is required to allow binding of protein substrates. The C-terminal helix bundle becomes mobile presumably after the melting of helix B opposite the substrate binding cavity, as suggested by amide hydrogen exchange data[36]. (ii) Allosteric regulation of the nucleotide-controlled chaperone activity requires a movement of helix A and the proximal part of helix B relative to the β subdomain. (iii) Interaction with folded protein substrates does not strictly require a closure of the helical lid. The paradigm that Hsp70-bound protein substrates interact with the chaperone through extended peptide stretches that are at least 10 Å separated from the folded portion of the substrate therefore has to be revised[6,10,37].

The SBD of Hsp70 chaperones must undergo large conformational rearrangements to allow substrate entry to the binding cavity. To differentiate between alternative possible movements, we introduced cysteine residues into DnaK based on the crystal structure of the DnaK SBD[10] with the aim of restricting the mobility of the helical lid relative to the β subdomain upon disulfide bond formation. Notably, binding of peptide as well as folded protein substrates is not affected by linking helix A or the proximal part of helix B to the β-sheet subdomain (**Fig. 2**). This finding strongly suggests that a melting of helix B opposite the substrate binding cavity as suggested in a previous study[10] (**Fig. 1c** left panel) can occur and is sufficient to allow entry of substrate molecules into the binding pocket.

Although the DnaK variants, which show a reduced mobility of the helical lid, bind to substrates similar to wild-type protein, they do not promote refolding of chemically denatured luciferase and they exhibit reduced chaperone activity toward heat-denatured MDH under oxidizing conditions (**Fig. 3** and **Supplementary Fig. 5**). This indicates that a different property of the protein is impaired, most likely allosteric control of the chaperone cycle by a nucleotide. Indeed, our data indicate that the transitions between the ATP- and ADP-bound states require a relocation of helix A relative to the β subdomain. DnaK-HA is clearly impaired in allosteric regulation in the oxidized state, as the protein is not responsive to stimulation of ATP hydrolysis by substrate and vice versa of peptide release by ATP (**Fig. 4**).

Our data indicate that there is an equilibrium between a 'lid closed' state, which is described by crystal structure determination[10] (gray structure in **Fig. 7a**); a 'lid open' state (lid between translucent green and translucent blue in **Fig. 7a**), where the spin labels do not interact in EPR; and an 'intermediate-open' conformation (translucent green in **Fig. 7a**), which is adopted upon binding to bulky substrates. According to our data, all three states are populated in the ADP-bound form, with the closed state being the prominent species. Upon ATP binding to the NBD, we detected only the open and intermediate-open conformations.

Hsp70s have several types of substrates (**Fig. 7b**): nascent chains at the ribosome and translocating polypeptides present themselves as largely unfolded substrates and, similar to peptide substrates, Hsp70s may completely encase them with the lid closed. However, Hsp70s also bind to native, stress denatured and aggregated proteins, which expose hydrophobic residues at the surface but which are unlikely in a completely extended conformation. In these cases, it is hard to imagine how the lid could thread between strands of an aggregate to enclose a single strand. Notably, amyloids contain β-sheet cores, and up to now it was inconceivable that Hsp70s could bind to these core structures, which would not allow a close encasement of a single strand. Our data give new insight into the interaction of Hsp70s with such structures and, consequently, the ambiguous role of Hsp70s in amyloid formation and prion propagation[38]. These findings imply that the range of Hsp70 target segments within protein substrates may be larger than anticipated from the crystal structure of the SBD of DnaK, which further broadens the functional versatility of Hsp70 chaperones in protein folding.

If the lid does not close on protein substrates, the question arises of why Hsp70s have this structural element. One possible explanation is that the lid contacts the substrate, as suggested by our cross-linking experiments (**Fig. 6**), and that this contact between the lid and substrate causes conformational changes in the substrate which are important for the chaperone action of Hsp70s. Indeed, the lidless DnaK variant DnaK163 was unable to refold chemically denatured firefly luciferase, suggesting that the lid may play an important role in the refolding of some substrates[30]. The lid may also directly interact with protein substrates to modulate the affinity for the substrate. Finally, the lid may also serve as a docking site for cochaperones. Eukaryotic Hsp70s have a number of TPR-domain–containing cochaperones such as Hop, Chip and TPR2 that bind to the C-terminal EEVD motif. Here the lid could have evolved into an interaction platform.

## METHODS

Methods and any associated references are available in the online version of the paper at http://www.nature.com/nsmb/.

*Note: Supplementary information is available on the Nature Structural & Molecular Biology website.*

ACKNOWLEDGMENTS

We are grateful to F. Rodriguez for providing RepE, C. Altenbach for providing the fitting software and T. Ruppert for mass spectrometry. We thank S. R. Scholz for critical reading of the manuscript and S. Miller for help with figure preparation. We thank CellNetworks for providing the FTIR spectrometer. This work was supported by the Deutsche Forschungsgemeinschaft (SFB638 and MA 1278/4-1 to M.P.M.) and a Kekulé fellowship of the Fonds der Chemischen Industrie to R.S.

AUTHOR CONTRIBUTIONS

R.S. designed, performed and interpreted the experiments in **Figures 2–4** and **Figure 6**, **Table 1**, **Supplementary Figures 1**,**4**,**5** and **9** and **Supplementary Table 1**. A.H.E. designed, performed and interpreted the experiments in **Figure 5** and **Supplementary Figures 6–8**. B.B. designed the experiments and supervised R.S. and A.H.E. M.P.M. designed all mutant proteins; designed, performed and interpreted experiments in **Supplementary Figure 2**; was involved in the design and interpretation of all experiments; and supervised R.S. and A.H.E. All authors prepared figures and wrote the manuscript.

COMPETING FINANCIAL INTERESTS

The authors declare no competing financial interests.

Published online at http://www.nature.com/nsmb/.
Reprints and permissions information is available online at http://npg.nature.com/reprintsandpermissions/.



1. Hartl, F.U. & Hayer-Hartl, M. Molecular chaperones in the cytosol: from nascent chain to folded protein. *Science* **295**, 1852–1858 (2002).
2. Mayer, M.P. & Bukau, B. Hsp70 chaperones: cellular functions and molecular mechanism. *Cell. Mol. Life Sci.* **62**, 670–684 (2005).
3. Bukau, B., Deuerling, E., Pfund, C. & Craig, E.A. Getting newly synthesized proteins into shape. *Cell* **101**, 119–122 (2000).
4. Gething, M.-J.H. & Sambrook, J.F. Protein folding in the cell. *Nature* **355**, 33–45 (1992).
5. Young, J.C., Agashe, V.R., Siegers, K. & Hartl, F.U. Pathways of chaperone-mediated protein folding in the cytosol. *Nat. Rev. Mol. Cell Biol.* **5**, 781–791 (2004).
6. Mayer, M.P., Rudiger, S. & Bukau, B. Molecular basis for interactions of the DnaK chaperone with substrates. *Biol. Chem.* **381**, 877–885 (2000).
7. Karzai, A.W. & McMacken, R. A bipartite signaling mechanism involved in DnaJ-mediated activation of the *Escherichia coli* DnaK protein. *J. Biol. Chem.* **271**, 11236–11246 (1996).
8. Liberek, K., Marszalek, J., Ang, D., Georgopoulos, C. & Zylicz, M. *Escherichia coli* DnaJ and GrpE heat shock proteins jointly stimulate ATPase activity of DnaK. *Proc. Natl. Acad. Sci. USA* **88**, 2874–2878 (1991).
9. McCarty, J.S., Buchberger, A., Reinstein, J. & Bukau, B. The role of ATP in the functional cycle of the DnaK chaperone system. *J. Mol. Biol.* **249**, 126–137 (1995).
10. Zhu, X. *et al.* Structural analysis of substrate binding by the molecular chaperone DnaK. *Science* **272**, 1606–1614 (1996).
11. Cupp-Vickery, J.R., Peterson, J.C., Ta, D.T. & Vickery, L.E. Crystal structure of the molecular chaperone HscA substrate binding domain complexed with the IscU recognition peptide ELPPVKIHC. *J. Mol. Biol.* **342**, 1265–1278 (2004).
12. Jiang, J., Prasad, K., Lafer, E.M. & Sousa, R. Structural basis of interdomain communication in the hsc70 chaperone. *Mol. Cell* **20**, 513–524 (2005).
13. Morshauser, R.C. *et al.* High-resolution solution structure of the 18 kDa substrate-binding domain of the mammalian chaperone protein Hsc70. *J. Mol. Biol.* **289**, 1387–1403 (1999).
14. Pellecchia, M. *et al.* Structural insights into substrate binding by the molecular chaperone DnaK. *Nat. Struct. Biol.* **7**, 298–303 (2000).
15. Stevens, S.Y., Cai, S., Pellecchia, M. & Zuiderweg, E.R. The solution structure of the bacterial HSP70 chaperone protein domain DnaK(393–507) in complex with the peptide NRLLLTG. *Protein Sci.* **12**, 2588–2596 (2003).
16. Wang, H. *et al.* NMR solution structure of the 21 kDa chaperone protein DnaK substrate binding domain: a preview of chaperone-protein interaction. *Biochemistry* **37**, 7929–7940 (1998).
17. Liu, Q. & Hendrickson, W.A. Insights into hsp70 chaperone activity from a crystal structure of the yeast Hsp110 Sse1. *Cell* **131**, 106–120 (2007).
18. Fernández-Sáiz, V., Moro, F., Arizmendi, J.M., Acebron, S.P. & Muga, A. Ionic contacts at DnaK substrate binding domain involved in the allosteric regulation of lid dynamics. *J. Biol. Chem.* **281**, 7479–7488 (2006).
19. Gisler, S.M., Pierpaoli, E.V. & Christen, P. Catapult mechanism renders the chaperone action of Hsp70 unidirectional. *J. Mol. Biol.* **279**, 833–840 (1998).
20. Schmid, D., Baici, A., Gehring, H. & Christen, P. Kinetics of molecular chaperone action. *Science* **263**, 971–973 (1994).
21. Vogel, M., Bukau, B. & Mayer, M.P. Allosteric regulation of Hsp70 chaperones by a proline switch. *Mol. Cell* **21**, 359–367 (2006).
22. Grossman, A.D., Straus, D.B., Walter, W.A. & Gross, C.A. $\sigma^{32}$ synthesis can regulate the synthesis of heat shock proteins in *Escherichia coli*. *Genes Dev.* **1**, 179–184 (1987).
23. Straus, D., Walter, W. & Gross, C.A. DnaK, DnaJ, and GrpE heat shock proteins negatively regulate heat shock gene expression by controlling the synthesis and stability of $\sigma^{32}$. *Genes Dev.* **4**, 2202–2209 (1990).
24. Tilly, K., McKittrick, N., Zylicz, M. & Georgopoulos, C. The DnaK protein modulates the heat-shock response of *Escherichia coli*. *Cell* **34**, 641–646 (1983).
25. Gamer, J., Bujard, H. & Bukau, B. Physical interaction between heat shock proteins DnaK, DnaJ, and GrpE and the bacterial heat shock transcription factor sigma 32. *Cell* **69**, 833–842 (1992).
26. Gamer, J. *et al.* A cycle of binding and release of the DnaK, DnaJ and GrpE chaperones regulates activity of the *Escherichia coli* heat shock transcription factor sigma32. *EMBO J.* **15**, 607–617 (1996).
27. Liberek, K., Galitski, T.P., Zylicz, M. & Georgopoulos, C. The DnaK chaperone modulates the heat shock response of *Escherichia coli* by binding to the $\sigma^{32}$ transcription factor. *Proc. Natl. Acad. Sci. USA* **89**, 3516–3520 (1992).
28. Liberek, K., Wall, D. & Georgopoulos, C. The DnaJ chaperone catalytically activates the DnaK chaperone to preferentially bind the $\sigma^{32}$ heat shock transcriptional regulator. *Proc. Natl. Acad. Sci. USA* **92**, 6224–6228 (1995).
29. Rodriguez, F. *et al.* Molecular basis for regulation of the heat shock transcription factor $\sigma^{32}$ by the DnaK and DnaJ chaperones. *Mol. Cell* **32**, 347–358 (2008).
30. Mayer, M.P. *et al.* Multistep mechanism of substrate binding determines chaperone activity of Hsp70. *Nat. Struct. Biol.* **7**, 586–593 (2000).
31. Buchberger, A. *et al.* Nucleotide-induced conformational changes in the ATPase and substrate binding domains of the DnaK chaperone provide evidence for interdomain communication. *J. Biol. Chem.* **270**, 16903–16910 (1995).
32. Moro, F., Fernandez, V. & Muga, A. Interdomain interaction through helices A and B of DnaK peptide binding domain. *FEBS Lett.* **533**, 119–123 (2003).
33. Altenbach, C., Oh, K.J., Trabanino, R.J., Hideg, K. & Hubbell, W.L. Estimation of inter-residue distances in spin labeled proteins at physiological temperatures: experimental strategies and practical limitations. *Biochemistry* **40**, 15471–15482 (2001).
34. Ishiai, M., Wada, C., Kawasaki, Y. & Yura, T. Replication initiator protein RepE of mini-F plasmid: functional differentiation between monomers (initiator) and dimers (autogenous repressor). *Proc. Natl. Acad. Sci. USA* **91**, 3839–3843 (1994).
35. Swain, J.F. *et al.* Hsp70 chaperone ligands control domain association via an allosteric mechanism mediated by the interdomain linker. *Mol. Cell* **26**, 27–39 (2007).
36. Rist, W., Graf, C., Bukau, B. & Mayer, M.P. Amide hydrogen exchange reveals conformational changes in hsp70 chaperones important for allosteric regulation. *J. Biol. Chem.* **281**, 16493–16501 (2006).
37. Rüdiger, S., Germeroth, L., Schneider-Mergener, J. & Bukau, B. Substrate specificity of the DnaK chaperone determined by screening cellulose-bound peptide libraries. *EMBO J.* **16**, 1501–1507 (1997).
38. Jones, G.W. & Tuite, M.F. Chaperoning prions: the cellular machinery for propagating an infectious protein? *Bioessays* **27**, 823–832 (2005).
39. Laufen, T. *et al.* Mechanism of regulation of hsp70 chaperones by DnaJ cochaperones. *Proc. Natl. Acad. Sci. USA* **96**, 5452–5457 (1999).

## ONLINE METHODS

**Plasmids.** The *dnaK* gene was PCR amplified from plasmid pUHE-2fdΔ12(*dnaK*$^{+}$)[40] (primers: 5′-CCAGTGGGTCTCAGGTGGTATGGGTAAAATAATTGGTATCG-3′; 5′-GGCCATCTCGAGTTATTTTTTGTCTTTGAC-3′), digested with BsaI and XhoI, and ligated into pCA528 (ref. 41), resulting in pCA528-*dnaK*. Double-cysteine mutants were constructed by site-directed mutagenesis[42].

**Proteins.** Wild-type and mutant DnaK were purified according to an established protocol[40] or fused to a N-terminal $His_6$-SUMO tag expressed from pCA528-*dnaK* in cells from the BL21 strain (Invitrogen) at 30 °C. The protein was purified using Ni-IDA matrix (Protino, Macherey-Nagel) and then washing with buffer A (25 mM HEPES-KOH, pH 7.6, 50 mM KCl and 5 mM EDTA) and buffer A containing 5 mM ATP. Protein was eluted with 250 mM imidazole and dialyzed against buffer A after supplementation with $His_6$-Ulp1. Disulfide bond formation was induced by diluting oxidizing solution (5 mM $CuSO_4$ and 17.5 mM 1,10-phenanthroline) ten times into a low concentration (<10 μM) protein solution and 10 min incubation at 30 °C. The catalyst was removed during nucleotide removal[43], and DnaK was further purified as described[40]. The nucleotide content (<3–5%) in the final protein preparation was assessed by analytical ion exchange chromatography[41]. $His_6$-$\sigma^{32}$ was purified as described previously[44], and $His_6$-RepE54 (RepE-R117P) was a kind gift of F. Rodriguez (Zentrum für Molekulare Biologie der Universität Heidelberg, Heidelberg, Germany).

**Kinetic measurements.** Kinetic measurements were performed at 30 °C in HKM buffer (25 mM HEPES-KOH, pH 7.6, 50 mM KCl and 5 mM $MgCl_2$). ATPase activities were determined under single-turnover conditions as described[45].

The dissociation rates for peptides were determined according to the procedure used in a previous study[30] with the modification of using dansyl-labeled NRLLLTG (DNR) peptide and unlabeled NRLLLTG (NR) peptide (Peptide Specialty Laboratories GmbH). Peptide association was determined by rapidly mixing 2 μM DNR peptide with 0.5 μM DnaK.

**Fluorescence spectra.** Measurements of the intrinsic tryptophan fluorescence were performed as described previously[30].

**Determination of dissociation constants.** Dissociation equilibrium constants for DnaK variants were determined as published[45]. The $K_d$ values were calculated by fitting a quadratic equation to the data using GraFit version 5.0 (Erithacus Software).

To determine the dissociation rate constants, 0.5 μM $^3$H-$\sigma^{32}$ and 5 μM DnaK were incubated at 30 °C for 2 h in a total volume of 20 μl. After addition of 1 mM NR peptide, the amount of complex remaining at different time points was determined by gel filtration. Rate constants were calculated by fitting a single exponential decay function to the data using GraFit version 5.0.

**Chaperone activity assays.** Refolding of chemically denatured luciferase was performed as published[46]. Malate dehydrogenase (MDH, 0.1 μM) was denatured at 47 °C for 30 min in MDH buffer (200 mM Tris, pH 7.5, 300 mM KCl and 40 mM magnesium acetate) in the presence of 0.1 μM DnaJ. Protein refolding was started by mixing MDH 1:1 with a chaperone solution (10 μM DnaK and 2 μM GrpE) at 30 °C. Enzymatic activity was measured by diluting aliquots 20 times into assay buffer (150 mM potassium phosphate pH 7.6, 0.5 mM oxaloacetate, 0.3 mM NADH and 1 mM DTT) and following the absorption of NADH in a microplate reader (FLUOstar Omega, BMG Labtech) at 340 nm for 5 min.

**Modification of cysteine residues and mass spectrometry.** The protein was incubated with a ten-fold excess of sodium (2-sulfonatoethyl)methanethiosulfonate (MTSES) over the total amount of thiols in the reaction. To probe the success of oxidation reactions, samples were treated in the presence of at least 5 M guanidine hydrochloride to ensure accessibility. Derivatized proteins were subjected to ESI-MS analysis on a QSTAR Pulsar (Applied Biosystems) mass spectrometer as described[36]. To separate $\sigma^{32}$ from DnaK, proteins were eluted from the trap column by a gradient from 40–75% buffer B within 35 min.

**Site-directed spin labeling.** DnaK single- and double-cysteine mutants were passed through a Spehadex G50 column equilibrated with buffer TKM (50 mM Tris-HCl, pH 7.6, 50 mM KCl and 5 mM $MgCl_2$) to remove the reducing agent and were immediately incubated with a ten-fold excess (over cysteine) of 1-oxyl-2,2,5,5-tetramethyl-Δ3-pyrroline-3-methyl methanethiosulfonate (MTSSL) to form a new side chain designated R1 (**Fig. 1a**). The free label was removed by gel filtration.

**EPR measurements.** All spectra were recorded with a Bruker ELEXSYS 500 cw X-Band spectrometer fitted with the Bruker ultra-high-sensitivity resonator (Super-High-Q Cavity: ER 4122SHQE, Bruker). The spectra were recorded as 200 Gauss (G) scans in solution at room temperature (22 °C) with an incident microwave power of 2 mW and modulation amplitude of 1.2 G at 100 kHz with DnaK concentrations of 50–100 μM. Spectra in the presence of ATP were recorded after addition of 2 mM ATP to the sample used to measure the spectra of nucleotide-free DnaK.

Peptide-DnaK complexes were pre-formed by incubating 50 μM spin-labeled DnaK with 300 μM peptide ($\sigma^{32}$-M195–Q207; MAPVLYLQDKSSN) at 30 °C for 1 h. To form $His_6$-$\sigma^{32}$ or $His_6$-RepE54-DnaK complexes, spin-labeled DnaK was diluted to 2 μM DnaK in buffer TKM and incubated with 10 μM substrate protein for 2 h at 30 °C. Unbound DnaK was removed by $Ni^{2+}$-NTA chromatography.

**Determination of interspin distances.** Interspin distance distributions were derived from spectra exhibiting broadening by spin-spin interactions of close spin label as described[33] using a software kindly provided by C. Altenbach using LabVIEW (National Instruments).

**Modeling of the R1 side chain in the structure of the DnaK SBD.** The R1 side chains were modeled into the DnaK SBD essentially as described in reference 47. The starting conformation for the R1 chains was $X_1 = 310°$ and $X_2 = 310°$ (g+g+ conformation)[48–50]. $X_3$ was also assigned g+ conformation (270°). The structure was energy minimized with all backbone Cβ and disulfide atoms fixed in space, allowing only rotations of the $X_4$ and $X_5$ dihedrals.

**Dissociation equilibrium titration.** We incubated 0.1 μM $\sigma^{32}$-Q132–Q144-C-AANS (ref. 51) with 0.05 to 5 μM wild-type DnaK and DnaK-E430R1, R547R1′ at 30 °C for 1 h. Fluorescence emission spectra (350–500 nm) were measured in a PerkinElmer LS55 Luminescence Spectrometer with a 335 nm excitation wavelength.

**Cross-linking.** DnaK-Q424C and DnaK-R547C were labeled with 4-(2-Iodoacetamido)benzophenone (BPIA), and cross-linking was performed as described[39]. Cross-linking mixtures contained 2 μM DnaK, 10 μM substrate ($His_6$-$\sigma^{32}$ or $His_6$-YFP) and 2 μM ATP.


40. Buchberger, A., Schroder, H., Buttner, M., Valencia, A. & Bukau, B. A conserved loop in the ATPase domain of the DnaK chaperone is essential for stable binding of GrpE. *Nat. Struct. Biol.* **1**, 95–101 (1994).
41. Andréasson, C., Fiaux, J., Rampelt, H., Mayer, M.P. & Bukau, B. Hsp110 is a nucleotide-activated exchange factor for Hsp70. *J. Biol. Chem.* **283**, 8877–8884 (2008).
42. Kunkel, T.A., Bebenek, K. & McClary, J. Efficient site-directed mutagenesis using uracil-containing DNA. *Methods Enzymol.* **204**, 125–139 (1991).
43. Theyssen, H., Schuster, H.P., Packschies, L., Bukau, B. & Reinstein, J. The second step of ATP binding to DnaK induces peptide release. *J. Mol. Biol.* **263**, 657–670 (1996).
44. Arsène, F. *et al.* Role of region C in regulation of the heat shock gene-specific sigma factor of *Escherichia coli*, $\sigma^{32}$. *J. Bacteriol.* **181**, 3552–3561 (1999).
45. Mayer, M.P., Laufen, T., Paal, K., McCarty, J.S. & Bukau, B. Investigation of the interaction between DnaK and DnaJ by surface plasmon resonance spectroscopy. *J. Mol. Biol.* **289**, 1131–1144 (1999).
46. Szabo, A. *et al.* The ATP hydrolysis-dependent reaction cycle of the *Escherichia coli* Hsp70 system DnaK, DnaJ, and GrpE. *Proc. Natl. Acad. Sci. USA* **91**, 10345–10349 (1994).
47. Altenbach, C., Cai, K., Klein-Seetharaman, J., Khorana, H.G. & Hubbell, W.L. Structure and function in rhodopsin: mapping light-dependent changes in distance between residue 65 in helix TM1 and residues in the sequence 306–319 at the cytoplasmic end of helix TM7 and in helix H8. *Biochemistry* **40**, 15483–15492 (2001).
48. Columbus, L., Kalai, T., Jeko, J., Hideg, K. & Hubbell, W.L. Molecular motion of spin labeled side chains in alpha-helices: analysis by variation of side chain structure. *Biochemistry* **40**, 3828–3846 (2001).
49. McHaourab, H.S., Lietzow, M.A., Hideg, K. & Hubbell, W.L. Motion of spin-labeled side chains in T4 lysozyme. Correlation with protein structure and dynamics. *Biochemistry* **35**, 7692–7704 (1996).
50. Langen, R., Oh, K.J., Cascio, D. & Hubbell, W.L. Crystal structures of spin labeled T4 lysozyme mutants: implications for the interpretation of EPR spectra in terms of structure. *Biochemistry* **39**, 8396–8405 (2000).
51. McCarty, J.S. *et al.* Regulatory region C of the *E. coli* heat shock transcription factor, $\sigma^{32}$, constitutes a DnaK binding site and is conserved among eubacteria. *J. Mol. Biol.* **256**, 829–837 (1996).





doi:10.1038/nsmb.2006